Type I interferon is a therapeutic target for virus-induced lethal vascular damage

Roberto Baccala[a,1], Megan J. Welch[a], Rosana Gonzalez-Quintial[a], Kevin B. Walsh[a,2], John R. Teijaro[a], Anthony Nguyen[a], Cherie T. Ng[a], Brian M. Sullivan[a], Alessandro Zarpellon[b], Zaverio M. Ruggeri[b], Juan Carlos de la Torre[a], Argyrios N. Theofilopoulos[a], and Michael B. A. Oldstone[a,1]

Departments of [a]Immunology and Microbial Science and [b]Molecular and Experimental Medicine, The Scripps Research Institute, La Jolla, CA 92037

Contributed by Michael B. A. Oldstone, May 5, 2014 (sent for review April 9, 2014)

The outcome of a viral infection reflects the balance between virus virulence and host susceptibility. The clone 13 (Cl13) variant of lymphocytic choriomeningitis virus—a prototype of Old World arenaviruses closely related to Lassa fever virus—elicits in C57BL/6 and BALB/c mice abundant negative immunoregulatory molecules, associated with T-cell exhaustion, negligible T-cell–mediated injury, and high virus titers that persist. Conversely, here we report that in NZB mice, despite the efficient induction of immunoregulatory molecules and high viremia, Cl13 generated a robust cytotoxic T-cell response, resulting in thrombocytopenia, pulmonary endothelial cell loss, vascular leakage, and death within 6–8 d. These pathogenic events required type I IFN (IFN-I) signaling on nonhematopoietic cells and were completely abrogated by IFN-I receptor blockade. Thus, IFN-I may play a prominent role in hemorrhagic fevers and other acute virus infections associated with severe vascular pathology, and targeting IFN-I or downstream effector molecules may be an effective therapeutic approach.

IFN-alpha | LCMV | platelet loss | immunopathology | lung

Lassa virus (LASV) is a hemorrhagic fever virus causing platelet malfunction, vascular permeability, and high mortality in a subset of patients (1). Endemic to West Africa, LASV ranks second in global incidence among hemorrhagic fever viruses, infects hundreds of thousands of individuals annually, and accounts for as many as 15% of hospital admissions in some areas (1, 2). Although most patients recover after a mild or asymptomatic course, ∼20% develop severe disease, culminating in >20,000 deaths per year. There is no licensed vaccine, and current therapy with ribavirin is limited because of toxicity. Further, the ease of spread and high mortality classifies LASV as a category A pathogen and bioterrorism threat.

The pathogenic mechanisms whereby LASV causes severe disease remain unclear. Studies in vitro with human cells and in vivo in nonhuman primates suggested reduced or delayed induction of type I IFNs (IFN-I), IFN-stimulated genes, and T-cell responses in fatal cases (1, 3–6). However, these studies are limited by the small number of animals examined and the lack of direct comparisons between responses in patients with severe vs. mild infections. Thus, it remains unknown how potential innate and adaptive immune dysfunctions might affect vascular integrity and disease severity.

To better understand innate and adaptive immune contributions to virus-induced vascular damage, we performed experiments in susceptible and resistant mice infected with lymphocytic choriomeningitis virus (LCMV). Like LASV, LCMV is an Old World arenavirus and serves as the prototype virus for this subgroup of the *Arenaviridae* family. Studies on LCMV have provided critical insights into Old World arenavirus virology, immunity, and pathogenesis, and led to the discovery of α-dystroglycan (α-DG), posttranslationally modified by the glycosyltransferase LARGE, as the cognate cellular receptor for both LCMV and LASV (7–10).

Here we show that, in susceptible mice, infection with certain variants of LCMV led to induction of a robust cytotoxic T-cell response refractory to negative regulation by inhibitory molecules, platelet loss, up-regulation of MHC class I (MHC-I) molecules by pulmonary endothelial cells, production of inflammatory cytokines and chemoattractants in the lungs, infiltration by activated T cells and inflammatory cells, severe vascular leakage, and death. All these manifestations were suppressed by IFN-I receptor (IFNAR) blockade, suggesting a novel molecular pathway that could be targeted in the treatment of hemorrhagic fevers and other viral conditions associated with lethal vascular injury.

Results and Discussion

The Cl13 Variant of LCMV Causes Lethal Vascular Leakage in NZB Mice. Two main classes of LCMV isolates have been described, represented by Armstrong (ARM; Cl 53b) and clone 13 (Cl13). Compared with ARM, Cl13 exhibits >100-fold higher affinity for α-DG, more efficiently infects dendritic cells (DCs) and macrophages, replicates at a faster rate in these cells, and reaches higher viremia in mice (11–15). Accordingly, i.v. inoculation of adult C57BL/6 or BALB/c mice with ARM induced an acute infection that was cleared within 8–12 d, whereas Cl13 established a persistent infection that lasted >60 d. In contrast, and consistent with an earlier study (16), infection of NZB mice with Cl13 caused a severe pathological response, indicated by reduced activity, ruffled fur, hunched posture, and labored breathing starting at day 4 postinfection (pi) and death of 100% of the mice

Significance

Lassa virus is, after dengue virus, the second most common cause of viral hemorrhagic fever. In susceptible individuals, Lassa virus infection is associated with vascular permeability, leading to tissue edema, organ failure, and death. Hemorrhagic fever viruses efficiently infect vascular endothelial cells, but are generally considered noncytopathic. Thus, the mechanism of virus-induced vascular injury remains unclear. Using the lymphocytic choriomeningitis virus variant clone 13, a prototype of Lassa virus, we show here that lethal vascular leakage in susceptible mice was completely prevented by type I IFN receptor blockade. Therefore, approaches that target type I IFNs or effector molecules induced by these cytokines may be considered for the treatment of Lassa fever and other severe hemorrhagic viral illnesses.

Author contributions: R.B. and M.B.A.O. designed research; R.B., M.J.W., R.G.-Q., K.B.W., J.R.T., A.N., C.T.N., B.M.S., and A.Z. performed research; J.C.d.l.T. contributed new reagents/analytic tools; Z.M.R., J.C.d.l.T., and A.N.T. contributed expertise; R.B., R.G.-Q., K.B.W., J.R.T., C.T.N., B.M.S., Z.M.R., J.C.d.l.T., A.N.T., and M.B.A.O. analyzed data; and R.B. and M.B.A.O. wrote the paper.

The authors declare no conflict of interest.

[1]To whom correspondence may be addressed. E-mail: mbaobo@scripps.edu or rbaccala@scripps.edu.

[2]Present address: Department of Molecular Biology, Genentech Inc, South San Francisco, CA 94080.

This article contains supporting information online at www.pnas.org/lookup/suppl/doi:10.1073/pnas.1408148111/-/DCSupplemental.

(73 of 73) between days 6 and 8 pi (Fig. 1*A*). Such manifestations were not observed in ARM-challenged NZB mice, all of which (18 of 18) survived the infection symptomless (Fig. 1*A*). Titers of Cl13 in serum were reduced (approximately sixfold) at day 4 pi and increased (~1.7-fold) at day 6 pi in NZB mice compared with BALB/c controls, whereas no significant differences were noted for ARM (Fig. S1). Histological examination of vital organs (lungs, heart, brain, liver, and kidney) on day 6 pi revealed that Cl13 induced pathological alterations primarily in the lungs, which showed marked pneumonitis, alveolar wall thickening, mononuclear cell infiltrate, and edema, consistent with the respiratory distress manifested by moribund mice (Fig. 1*B*). In contrast, these histopathological changes were absent in ARM-infected NZB mice (Fig. 1*B*), as well as in Cl13-infected C57BL/6 and BALB/c mice (Fig. S2). Vascular permeability leading to pulmonary edema was confirmed and quantified by the elevated leakage of i.v.-administered Evan's blue in the lungs of NZB mice 5 d after Cl13, but not ARM, infection (Fig. 1*C*). As an additional indicator of potential vascular abnormalities, Cl13-infected NZB mice had significantly reduced platelet counts compared with ARM-infected and control mice (Fig. 1*D*). Thus, NZB mice infected with Cl13 exhibited an acute disease associated with thrombocytopenia, vascular leakage, and mortality, characteristics typical of severe Lassa fever (LF) and other hemorrhagic fevers.

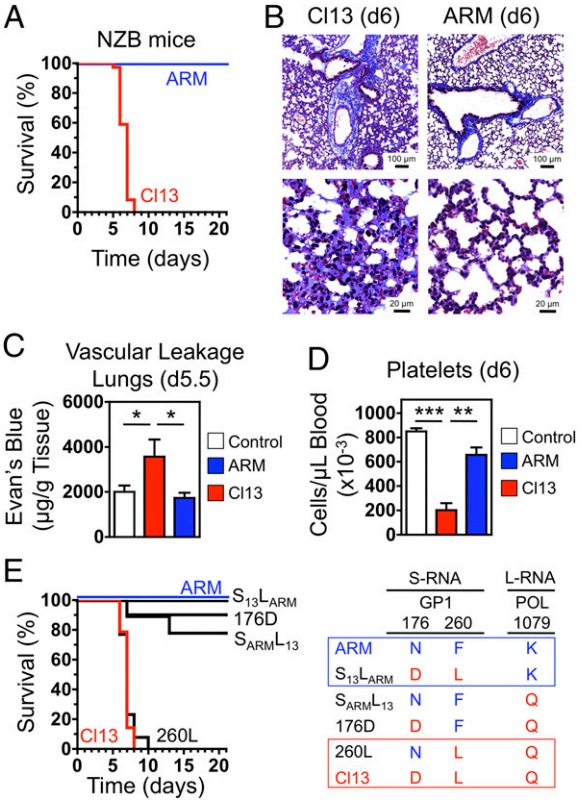

Fig. 1. LCMV Cl13 causes lethal vascular leakage in NZB mice. (*A*) NZB mice were infected i.v. with 2×10^6 PFU of either Cl13 ($n = 73$) or ARM ($n = 18$). The Kaplan–Meier survival plot summarizes data from 19 experiments with Cl13 and 5 experiments with ARM. (*B*) Histochemical analysis (Masson's trichrome) of lung sections from Cl13- or ARM-infected NZB mice ($n = 3$ or 4 per group) on day 6 pi. Data are representative of three independent experiments. [Scale bars, 100 μm (*Upper*) or 20 μm (*Lower*).] (*C*) Vascular leakage in infected and control NZB mice ($n = 3$ per group) assessed on day 5.5 pi by quantification of Evan's blue dye retained in perfused lungs 20 min after i.v. injection. Data are representative of two independent experiments (average ± SEM; Student *t* test). (*D*) Blood platelet counts in infected and control NZB mice ($n = 5$ per group) on day 6 pi. Data are from two independent experiments (average ± SEM; Student *t* test). (*E*) Residues 260L of the glycoprotein GP1 and 1079Q of the RNA polymerase POL are critical for the pathogenicity of Cl13 in NZB mice. Mice were infected with Cl13 ($n = 14$), ARM ($n = 13$), or the recombinant viruses $S_{13}L_{ARM}$ ($n = 10$), $S_{ARM}L_{13}$ ($n = 9$), 176D ($n = 10$), or 260L ($n = 13$). The Kaplan–Meier survival plot summarizes data from three or four experiments. Significant differences are indicated. $^*P < 0.05$; $^{**}P < 0.005$; $^{***}P < 0.0005$.

Mutations in the Virus That Enhance Infection of α-DG–Expressing Cells and Viral Replication Are Critical for the Pathogenicity of Cl13 in NZB Mice. ARM and Cl13 differ only at three amino acid positions: F260L and N176D in the glycoprotein GP1, and K1079Q in the L polymerase (POL). F260L in GP1 confers enhanced affinity of Cl13 to α-DG and facilitates virus binding and entry into DCs, the cell type that expresses >98% of α-DG located on immune cells (11, 14, 15, 17, 18); K1079Q in the L polymerase promotes enhanced (~100-fold) Cl13 multiplication in DCs (15, 18); conversely, N176D in GP1 does not play a significant role on the establishment of infection (14, 15). To elucidate the role of these amino acid residues in the lethal disease caused by Cl13 in NZB mice, we used four recombinant LCMV (rLCMV) variants (Fig. 1*E*) generated by reverse genetics (19). The rLCMV $S_{13}L_{ARM}$, expressing POL-1079K (as in ARM) along with GP1-260L and GP1-176D (both as in Cl13), behaved like ARM and induced no pathology in these mice (Fig. 1*E*). The rLCMV 176D and $S_{ARM}L_{13}$, both displaying POL-1079Q (as in Cl13) and GP1-260F (as in ARM) but differing in position GP1-176, were slightly more pathogenic than ARM and induced death in only 10–20% of the mice, respectively (Fig. 1*E*). In contrast, the rLCMV 260L, expressing POL-1079Q and GP1-260L (both as in Cl13) along with GP1-176N (as in ARM), was as pathogenic as Cl13 and induced death in all mice by day 10 pi (Fig. 1*E*). Importantly, the degree of pathogenicity mediated by each of these rLCMVs in NZB mice correlated with the degree of viremia and persistence induced in C57BL/6 mice (14, 15). These results indicate that cell tropism and magnitude of viral load are both critical for the Cl13-induced disease in NZB mice, and residues 260 and 1079 in GP1 and L polymerase, respectively, are key viral genetic determinants of pathogenicity.

Cl13 Induces in NZB Mice a Pathogenic Cytotoxic T-Cell Response Refractory to Negative Immunoregulation. The persistent infection established by Cl13 in C57BL/6 or BALB/c mice is associated with induction of an immunosuppressive state, characterized by production of inhibitory cytokines, such as interleukin-10 (IL-10) and IFN-I, and up-regulation of inhibitory receptors on effector T cells, such as programmed cell death 1 (PD-1), T cell immunoglobulin and mucin domain 3 (TIM-3), and lymphocyte activation gene 3 (LAG-3), leading to T-cell exhaustion (20–25). Induction of T-cell exhaustion is part of a physiological program aimed at limiting immunopathology caused by excessive and protracted immune responses and high antigen/virus load (23–26). Strikingly, unlike C57BL/6 (H-2^b) or BALB/c (H-2^d) mice, NZB mice (H-2^d) mounted a robust cytotoxic T-cell response to Cl13 that, at day 6 pi, was almost as efficient as in ARM-challenged controls (Fig. 2*A*). Lysis was noted with isologous, but not heterologous, ^{51}Cr-labeled infected target cells (Table S1). In addition, increased cytotoxic T lymphocyte (CTL) activity in Cl13-infected NZB mice compared with BALB/c mice correlated with enhanced frequency of virus-specific (H-2^d/LCMV-$NP_{118–126}$-tetramer$^+$) $CD8^+$ T cells that also displayed heightened T-cell receptor density and/or affinity, as illustrated by the intensity of MHC/peptide tetramer staining (Fig. 2*B*). These virus-specific NZB T cells exhibited multiple effector functions, indicated by the expression of granzyme B, IFN-γ, or both IFN-γ and TNF-α (Fig. 2*C*), an activated phenotype ($CD44^{hi}CD62L^{low}$), and up-regulation of the costimulatory molecule CD137 (4-1BB), known to

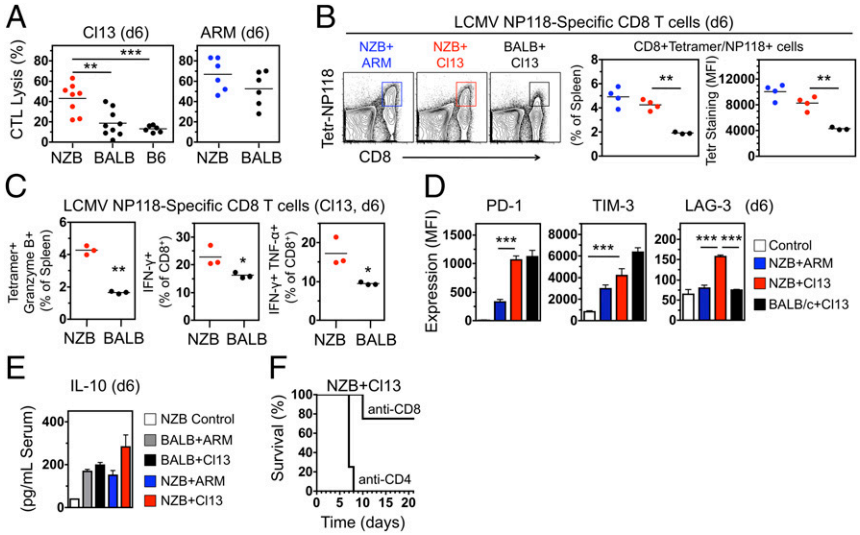

Fig. 2. Cl13 pathogenicity in NZB mice correlates with induction of a robust T-cell response resistant to negative immunoregulation. (*A*) Virus-specific CTL activity in spleen of infected mice (day 6 pi) examined in vitro by using Cl13-infected BALB/Cl7 (H-2^d, for NZB and BALB/c mice) or MC57 (H-2^b, for C57BL/6 mice) cell targets. Data are from two or three independent experiments (n = 6–9 mice per group; Student t test). (*B*, *Left*) FACS analysis of spleen cells (ARM-infected NZB mice and Cl13-infected NZB and BALB/c mice, day 6 pi) stained with anti-CD8 antibody and MHC/peptide tetramer (H-2^d/LCMV-NP$_{118–126}$) to identify virus-specific T cells. (*Center*) Frequency of virus-specific T cells (identified by FACS as in *Left*). (*Right*) Binding efficiency of MHC/peptide–tetramer to virus-specific T cells (identified as in *Left*), determined by FACS and expressed as mean fluorescence intensity (MFI). Data are representative of two independent experiments (n = 3 or 4 mice per group; Student t test). (*C*, *Left*) Frequency of virus-specific T cells (CD8$^+$MHC/peptide–tetramer$^+$) expressing granzyme B in spleen (day 6 pi), as determined by FACS. (*Center* and *Right*) Frequency of virus-specific CD8$^+$ T cells producing IFN-γ or both IFN-γ and TNF-α in spleen of Cl13-infected mice (day 6 pi), as determined by FACS after in vitro restimulation with LCMV–NP$_{118–126}$. Data are representative of two independent experiments (n = 3 mice per group; Student t test). (*D*) Expression of the inhibitory molecules PD-1 (*Left*), TIM-3 (*Center*), and LAG-3 (*Right*) by virus-specific T cells (CD8$^+$MHC/peptide–tetramer$^+$) in spleen of control and infected mice (day 6 pi), assessed by FACS and shown as MFI (average ± SEM; n = 4 mice per group; Student t test). (*E*) Serum IL-10 levels (day 6 pi) determined by ELISA (average ± SEM; n = 4 mice per group; Student t test). (*F*) Survival of Cl13-infected NZB mice treated with depleting anti-CD8 or -CD4 antibodies (n = 4 per group). Significant differences are indicated. *P < 0.05; **P < 0.005; ***P < 0.0005.

promote granzyme B expression. Remarkably, acquisition of inhibitory receptors by virus-specific T cells in Cl13-infected NZB mice was as efficient as in BALB/c mice for PD-1 and TIM-3, and more efficient for LAG-3 (Fig. 2*D*). Moreover, serum IL-10 levels were significantly elevated in NZB and BALB/c mice infected with either Cl13 or ARM, with the highest levels observed in Cl13-infected NZB mice (Fig. 2*E*). Despite the expression of these negative regulatory molecules, the cytotoxic T cells generated in Cl13-infected NZB mice failed to become functionally exhausted and, instead, robustly contributed to disease progression, because depletion of CD8$^+$, but not CD4$^+$, T cells significantly reduced disease and extended survival (Fig. 2*F* and Fig. S3). Thus, the anticipated immunosuppressive program was efficiently induced in Cl13-infected NZB mice but did not prevent the development of killer CD8$^+$ T cells, resulting in severe immune-mediated injury.

Cl13 Pathogenicity in NZB Mice Requires Toll-Like Receptor-Independent Production of IFN-α and Is Abrogated by IFNAR Blockade. A cardinal event in the response to most viruses is the early production of high levels of IFN-I. These pleiotropic cytokines are known to ignite a signaling cascade culminating in the expression of multiple costimulatory, proinflammatory, and survival factors necessary for an efficient antiviral response (27). However, IFN-I has recently been shown to also exert proviral effects, by promoting expression of negative regulatory molecules, leading to T-cell exhaustion and suppression of antiviral responses (24, 25). We hypothesized that the balance between immunostimulatory and immunosuppressive functions of IFN-I may be altered in some genetically predisposed individuals who, like Cl13-infected NZB mice, develop abnormal antiviral responses associated with severe immunopathology. Serum IFN-α levels and kinetics during the first 6 d pi were similar between Cl13- and ARM-infected NZB mice (Fig. S4). Remarkably, however, treatment with a blocking antibody to the IFN-I receptor (IFNAR) during the acute phase of the infection, beginning as late as 1 d pi, completely prevented disease manifestations, resulting in 100% (14 of 14) survival of Cl13-infected NZB mice (Fig. 3*A* and Fig. S5). Treatment efficacy decreased thereafter—i.e., 30% survival when initiated 60 h pi and 0% when initiated 72 h pi (Fig. S5). After antibody treatment discontinuation, all surviving mice remained free of virus-induced symptoms until they were killed, up to 1 y pi, despite carrying high titers [10^4–10^5 plaque-forming units (PFU) per mL of serum] of infectious virus. Complete protection from Cl13-mediated acute immunopathology was also observed in congenic *Ifnar1*$^{-/-}$ NZB mice lacking the α-chain of IFNAR, whereas all *Ifnb*$^{-/-}$ NZB mice succumbed by day 6 pi (Fig. 3*B*), indicating that IFN-α signaling is sufficient for disease induction.

We next investigated the innate pathways involved in pathogenic IFN-I production. Previous studies in C57BL/6 mice showed that induction of these cytokines by LCMV is mediated by viral RNA engagement of both endosomal Toll-like receptors (TLRs) and cytosolic RNA sensors (RIG-I and MDA5) (28–32). We found that congenic NZB mice lacking either expression of TLR3 (*Tlr3*$^{-/-}$), or signaling by all endosomal TLRs (TLRs 3, 7, and 9) due to the *3d* mutation of UNC93B1 (*Unc93b1*$^{3d/3d}$) (33), succumbed to Cl13 infection unless treated with IFNAR-blocking antibody (Fig. 3*C*). These data indicate that the endosomal TLR pathway is not necessary for pathogenic IFN-α production in Cl13-infected NZB mice and that the RIG-I/MDA5–dependent pathway appears to be sufficient for mediating the lethal outcome.

IFNAR Blockade Suppresses the Cytotoxic T-Cell Response and Prevents Platelet Loss in Cl13-Infected NZB Mice. The beneficial effect of IFNAR blockade in Cl13-infected NZB mice was not

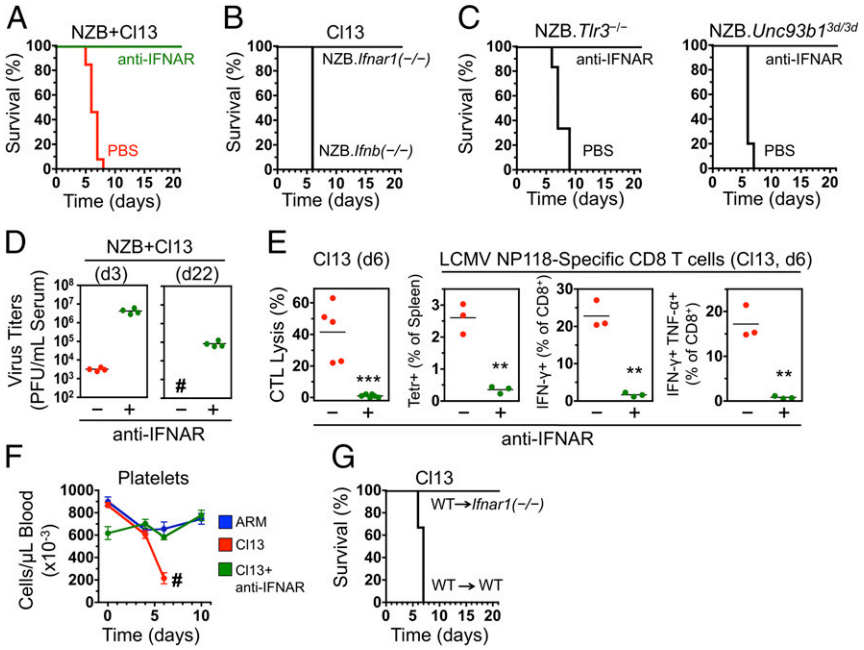

Fig. 3. Cl13 pathogenicity in NZB mice requires TLR-independent IFN-α production and IFNAR signaling on nonhematopoietic cells. (*A*) Survival of Cl13-infected NZB mice treated with anti-IFNAR antibody ($n = 14$) or PBS ($n = 13$), starting 1 d before infection. Data are from four independent experiments. (*B*) Survival of Cl13-infected NZB.*Ifnar1*$^{-/-}$ ($n = 8$) and NZB.*Ifnb*$^{-/-}$ ($n = 5$) congenic mice. Data are from two independent experiments. (*C*) Survival of Cl13-infected NZB.*Tlr3*$^{-/-}$ (*Left*) and NZB.*Unc93b1*$^{3d/3d}$ (lacking signaling by the endosomal TLRs 3, 7, and 9; *Right*) congenic mice treated with PBS ($n = 5$ or 6 mice) or IFNAR-blocking antibody ($n = 4$). (*D*) Virus titers in blood of Cl13-infected NZB mice treated or not with anti-IFNAR antibody ($n = 4$ per group) and analyzed at days 3 (*Left*) and 22 (*Right*) pi. #All untreated mice died on day 7 pi and could not be analyzed at day 22. (*E*) NZB mice were treated or not with IFNAR-blocking antibody starting 1 d before infection. CTL activity and frequencies of virus-specific and cytokine-producing T cells were assessed on day 6 pi, as specified in Fig. 2 *A*–*C*. Data are representative of two independent experiments ($n = 3$–5 mice per group; Student *t* test). (*F*) Blood platelet counts in ARM-infected ($n = 5$), Cl13-infected ($n = 8$), and Cl13-infected and treated with anti-IFNAR ($n = 8$) NZB mice. #Of the Cl13-infected but untreated mice, two died on day 6 and six on day 7. Data are from two independent experiments (average ± SEM). (*G*) Survival of Cl13-infected bone marrow chimeras generated between WT and *Ifnar1*$^{-/-}$ NZB mice ($n = 4$ per group). Significant differences are indicated. $^{**}P < 0.005$; $^{***}P < 0.0005$.

due to earlier resolution of the infection, because virus titers were significantly increased (~1,000-fold) 3 d pi in antibody-treated compared with control mice (Fig. 3*D*), likely due to the loss of IFN-I antiviral effects. Disease inhibition correlated with complete suppression of the cytotoxic response (Fig. 3*E*), consistent with disease reduction in CD8$^+$ T-cell–depleted mice (see above) and reflecting the crucial role of IFN-I in promoting virus-specific T-cell activation, proliferation, and survival (27). In addition, IFNAR blockade prevented platelet loss occurring in Cl13-infected NZB mice (Fig. 3*F*), a finding likely related to the negative effects of IFN-I signaling on megakaryocyte maturation, platelet production, and function (34–37).

IFN-I Signaling on Nonhematopoietic Cells Is Critical for Pathogenicity in Cl13-Infected NZB Mice. To determine whether IFN-I signaling on hematopoietic cells (particularly CD8$^+$ T cells, antigen-presenting cells, and megakaryocytes) was sufficient to explain the disease-promoting effect, we generated bone marrow chimeras between wild-type (WT) and *Ifnar1*$^{-/-}$ NZB mice. Strikingly, unlike WT→WT controls, WT→*Ifnar1*$^{-/-}$ chimera, in which bone marrow-derived cells, but not parenchymal cells, can respond to IFN-I, survived Cl13 infection (Fig. 3*G*). Thus, the lethal effects of Cl13 in NZB mice can be abrogated by interrupting IFNAR signaling in nonhematopoietic cells.

IFN-I Signaling Promotes Cytokine Production, Inflammatory Cell Infiltration, Endothelial Cell Loss, and Severe Vascular Leakage in Lungs of Cl13-Infected NZB Mice. The pathogenic relevance of IFN-I signaling in parenchymal cells prompted us to examine the consequences of IFNAR blockade in lungs, the organ primarily affected in this model. Vascular leakage, assessed by measuring extravasation of i.v. Evan's blue, was completely inhibited in lungs of Cl13-infected NZB mice treated with IFNAR-blocking antibody (Fig. 4 *A* and *B*). Similarly, analysis of bronchoalveolar lavage fluid (BALF) showed significant increases in total protein, lactate dehydrogenase, and IgM exudates in the airways of Cl13-infected NZB mice compared with ARM-infected or noninfected controls, and these indicators of vascular hyperpermeability were also corrected by IFNAR blockade (Fig. 4*C*). Cl13 infected 62% of lung vascular endothelial cells compared with <1% infected by ARM (Fig. 4*D*), consistent with the binding of Cl13 to α-DG, highly expressed by these cells (7, 9, 11, 38). IFNAR antibody treatment did not inhibit, but rather enhanced, endothelial cell infection, likely due to the absence of antiviral effects mediated by IFN-I signaling (Fig. 4*D*). IFNAR blockade also had no effect on the expression of the inhibitory molecule PD-L1, which was strongly up-regulated in Cl13-infected endothelial cells in both treated and nontreated mice (Fig. S6). IFNAR blockade, however, significantly inhibited MHC-I up-regulation and endothelial cell loss in Cl13-infected NZB mice (Fig. 4*E*), which correlated with reduced lung infiltration of multifunctional (IFN-γ$^+$TNF-α$^+$) CD8$^+$ T cells (Fig. 4*F*). Moreover, infiltration of activated macrophages, natural killer (NK) cells, and total leukocytes, significantly elevated in Cl13-infected NZB mice, was also suppressed by IFNAR blockade (Fig. 4*G*), as was local production of chemoattractants and cytokines (CCL2, CCL5, and TNF-α) assessed by BALF analysis (Fig. 4*H*). In contrast, in nonsusceptible BALB/c mice, Cl13 infected >80% of lung endothelial cells and caused significant up-regulation of MHC-I, but endothelial cell loss was not observed (Fig. S7), consistent with the paucity of cytotoxic T-cell effectors induced by Cl13 in these mice (Fig. 2). These data indicate that in susceptible mice

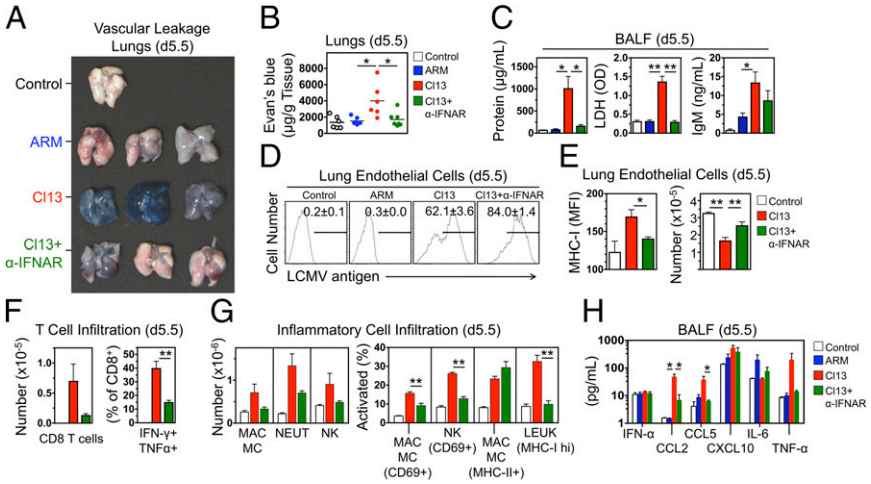

Fig. 4. IFNAR-dependent vascular leakage, endothelial cell loss, and inflammatory cell infiltration in lungs of Cl13-infected NZB mice. (*A*) NZB mice were treated or not with anti-IFNAR antibody (1 d before infection), infected with either Cl13 or ARM, and injected i.v. on day 5.5 pi with Evan's blue. Perfused lungs were harvested 20 min later. Images are representative of two independent experiments ($n = 3$ mice per group). (*B*) Evan's blue levels in lungs (obtained as described in *A*) at day 5.5 pi were quantified. Data are from two independent experiments ($n = 6$ mice per group; Student *t* test). (*C*) Protein, lactate dehydrogenase (LDH), and IgM exudates in airways of control and infected NZB mice, as assessed by BALF analysis at day 5.5 pi (average ± SEM; $n = 3$ or 4 mice per group; Student *t* test). (*D*) Intracellular LCMV in lung vascular endothelial cells ($CD45^-CD31^+$Podoplanin/$gp38^-$) at day 5.5 pi detected by FACS. Numbers indicate frequencies (average ± SEM) of infected cells ($n = 3$ or 4 mice per group). (*E*) Lung endothelial cells ($CD45^-CD31^+$ Podoplanin/$gp38^-$) at day 5.5 pi were enumerated, and MHC-I expression was quantified (MFI) by FACS (average ± SEM; $n = 3$ or 4 mice per group; Student *t* test). (*F*) Lung infiltration by virus-specific, IFN-γ^+TNF-α^+ $CD8^+$ T cells was assessed by FACS at day 5.5 pi (average ± SEM; $n = 3$ or 4 mice per group; Student *t* test). (*G*) Lung infiltration by activated leukocytes (LEUK, $CD45^+$, MHC-I^{hi}), macrophages/monocytes (MAC/MC, $CD11b^+F4/80^+Ly6G^-$, $CD69^+$ or MHC-II^+), and NK cells ($NK1.1^+CD3^-$, $CD69^+$) assessed by FACS at day 5.5 pi (average ± SEM; $n = 4$ mice per group; Student *t* test). (*H*) Levels of chemokines and cytokines in BALF (day 5.5 pi) assessed by ELISA (average ± SEM; $n = 3$ or 4 mice per group; Student *t* test). Significant differences are indicated. $*P < 0.05$; $**P < 0.005$.

IFN-I signaling on infected lung endothelial cells initiates a chain of events—including up-regulation of MHC-I, production of cytokines and chemokines, and recruitment of activated cytotoxic T cells and inflammatory cells—that rapidly lead to endothelial cell loss, vascular permeability, edema, and death in predisposed mice, all of which is suppressed by IFNAR antibody treatment.

Conclusions

Using variants of LCMV and mice with different degrees of susceptibility, we demonstrate that IFN-I critically contributes to virus-induced vascular damage and death—major characteristics of LF and other severe hemorrhagic viral diseases. Highlighting the relevance of both virus and host genetics, lethality in this model correlated with both the efficacy of virus replication in DCs, macrophages, and vascular endothelial cells, and the strength of the host cytotoxic T-cell response, which was IFN-I–dependent and resistant to immunoregulatory signals. In addition to NZB mice, preliminary experiments showed similar lethality following Cl13 infection in PL/J and SJL strains of mice. These results suggest that diverse outcomes in susceptible and resistant individuals may reflect differences in virus strain pathogenicity, T-cell response efficiency, and IFN-I–mediated immunoregulation. Although IFN-I has long been thought to protect the host from viral infections due to potent antiviral and immune response-promoting effects, recent studies have implicated these cytokines in harming the host in a number of viral and bacterial infections (24, 25, 39, 40). The present study provides an additional example of the detrimental contributions of IFN-I during antiviral responses. Defining the molecular mechanisms controlling the switch between beneficial and hurtful effects of IFN-I may therefore have a critical impact on the understanding of antiviral immune responses and susceptibility to immunopathology. Similar to our results with Cl13-infected NZB mice, the pathogenic role of T cells was recently demonstrated in LASV-infected transgenic mice expressing human MHC-I molecules (41). Whether severe LF in humans is also associated with a pathogenic T-cell response remains unknown. Robust in vitro memory $CD4^+$ T-cell responses to LASV in antibody-seropositive surviving individuals suggested that efficient T-cell immunity develops during nonfatal infections (42). However, studies that measure the potency of T-cell responses or IFN-I levels in patients with lethal LF have not been reported (3–6). We also noted that fatal vascular leakage in Cl13-infected NZB mice correlated with IFN-I–dependent platelet loss. Whether this finding is a cause or a consequence of disease remains to be clarified. In a different virus infection model, platelet loss was also prevented in the absence of IFNAR signaling (34). Interestingly, lethal disease in Cl13-infected NZB mice required IFN-I signaling in nonhematopoietic cells, as well as efficient infection of endothelial cells, which showed IFN-I–dependent up-regulation of MHC-I and decreased cellularity. Because endothelial cells are also key mediators of inflammatory responses (43), these events are likely critical for recruitment of immune cells and vascular injury. Like LCMV–Cl13, LASV and other hemorrhagic fever viruses infect endothelial cells, but these viruses are rarely cytopathic, implicating the immune response as the mechanism of vascular leakage (3, 4). Although blockade of PD-1/PD-L1 engagement has been shown to cause CTL-mediated killing of infected endothelial cells (26), we show here that in susceptible mice $CD8^+$ T-cell–mediated endothelial damage can occur even when these inhibitory molecules are efficiently up-regulated. Further investigation will be required to clarify why cytotoxic T cells can remain refractory to immunoregulation, how IFN-I signaling contributes to platelet loss and dysfunction, whether IFN-I activates different sets of genes in susceptible vs. resistant mice, and the precise molecular mechanisms involved in IFN-I–dependent vascular pathogenesis. In addition, the relevance of these findings for humans with severe virus-induced hemorrhagic diseases should be assessed, especially the role of IFN-I and its signaling.

Materials and Methods

Mice were infected by i.v. injection of 2×10^6 PFU of Cl13, ARM, or rLCMV variants generated by reverse genetics (15, 19). IFNAR blockade was accomplished by treating mice intraperitoneally with the monoclonal anti-IFNAR antibody MAR1-5A3 (Leinco Technologies) as described (44), by using 500 μg at the first injection (given 1 d before infection unless otherwise specified), followed by 250 μg three times per week for up to 2 wk. For $CD4^+$ or $CD8^+$ T-cell depletion, mice were treated with the monoclonal antibodies GK1.5 or YTS69, respectively (500 μg on days −1 and 0, and 250 μg on days 3 and 5 pi). Vascular leakage was assessed by i.v. injection of 200 μL of Evan's blue dye (0.5% in PBS), followed 20 min later by lethal anesthesia, perfusion by intracardial PBS injection, lung harvest, extraction of Evan's blue by overnight incubation in formamide at 56 °C, and quantitation by photometrical analysis (620 nm). CTL activity in infected mice was assessed by incubating spleen cells with infected, ^{51}Cr-labeled MC57 (H-2^b), or BALB/Cl7 (H-2^d) target cells at the effector-to-target ratio of 50:1. Virus-specific T cells were analyzed by FACS using MHC-I tetramers (H-$2L^d$/ $NP_{118–126}$). Cytokine production by virus-specific T cells was determined by FACS analysis of spleen cells restimulated in vitro with the LCMV peptide $NP_{118–126}$ (2 mg/mL) in the presence of brefeldin A (4 mg/mL) and stained intracellularly with antibodies to IFN-γ (XMG1.2) and TNF-α (MP6 XT22). For statistical analysis, groups were compared by unpaired two-tailed Student *t* test, and survival was analyzed by Kaplan–Meier plot and log-rank test ($P < 0.05$ was considered significant). Additional details on virus variants, mouse strains, bone marrow chimera, tissue and cell isolation, vascular leakage and BALF analyses, CTL assay, ELISA, and FACS can be found in *SI Materials and Methods*.

ACKNOWLEDGMENTS. This work was supported by National Institutes of Health Research Grants AI099699 and AI009484 (to M.B.A.O.), CA127535 (to R.B.), AR53228 (to A.N.T.), AI077719 (to J.C.d.l.T.), and HL42846 (to Z.M.R.). This is Publication 26053 of The Scripps Research Institute, Department of Immunology and Microbial Science.

1. McCormick JB, Fisher-Hoch SP (2002) Lassa fever. *Curr Top Microbiol Immunol* 262: 75–109.
2. Ogbu O, Ajuluchukwu E, Uneke CJ (2007) Lassa fever in West African sub-region: An overview. *J Vector Borne Dis* 44(1):1–11.
3. Russier M, Pannetier D, Baize S (2012) Immune responses and Lassa virus infection. *Viruses* 4(11):2766–2785.
4. Paessler S, Walker DH (2013) Pathogenesis of the viral hemorrhagic fevers. *Annu Rev Pathol* 8:411–440.
5. Koma T, Huang C, Kolokoltsova OA, Brasier AR, Paessler S (2013) Innate immune response to arenaviral infection: A focus on the highly pathogenic New World hemorrhagic arenaviruses. *J Mol Biol* 425(24):4893–4903.
6. Zapata JC, et al. (2013) Transcriptome analysis of human peripheral blood mononuclear cells exposed to Lassa virus and to the attenuated Mopeia/Lassa reassortant 29 (ML29), a vaccine candidate. *PLoS Negl Trop Dis* 7(9):e2406.
7. Cao W, et al. (1998) Identification of alpha-dystroglycan as a receptor for lymphocytic choriomeningitis virus and Lassa fever virus. *Science* 282(5396):2079–2081.
8. Kanagawa M, et al. (2004) Molecular recognition by LARGE is essential for expression of functional dystroglycan. *Cell* 117(7):953–964.
9. Kunz S, et al. (2005) Posttranslational modification of alpha-dystroglycan, the cellular receptor for arenaviruses, by the glycosyltransferase LARGE is critical for virus binding. *J Virol* 79(22):14282–14296.
10. Oldstone MB, Campbell KP (2011) Decoding arenavirus pathogenesis: Essential roles for alpha-dystroglycan-virus interactions and the immune response. *Virology* 411(2): 170–179.
11. Sevilla N, et al. (2000) Immunosuppression and resultant viral persistence by specific viral targeting of dendritic cells. *J Exp Med* 192(9):1249–1260.
12. Ahmed R, Salmi A, Butler LD, Chiller JM, Oldstone MB (1984) Selection of genetic variants of lymphocytic choriomeningitis virus in spleens of persistently infected mice. Role in suppression of cytotoxic T lymphocyte response and viral persistence. *J Exp Med* 160(2):521–540.
13. Ahmed R, Oldstone MB (1988) Organ-specific selection of viral variants during chronic infection. *J Exp Med* 167(5):1719–1724.
14. Bergthaler A, et al. (2010) Viral replicative capacity is the primary determinant of lymphocytic choriomeningitis virus persistence and immunosuppression. *Proc Natl Acad Sci USA* 107(50):21641–21646.
15. Sullivan BM, et al. (2011) Point mutation in the glycoprotein of lymphocytic choriomeningitis virus is necessary for receptor binding, dendritic cell infection, and long-term persistence. *Proc Natl Acad Sci USA* 108(7):2969–2974.
16. Puglielli MT, et al. (1999) Reversal of virus-induced systemic shock and respiratory failure by blockade of the lymphotoxin pathway. *Nat Med* 5(12):1370–1374.
17. Salvato M, Borrow P, Shimomaye E, Oldstone MB (1991) Molecular basis of viral persistence: A single amino acid change in the glycoprotein of lymphocytic choriomeningitis virus is associated with suppression of the antiviral cytotoxic T-lymphocyte response and establishment of persistence. *J Virol* 65(4):1863–1869.
18. Lee AM, Cruite J, Welch MJ, Sullivan B, Oldstone MB (2013) Pathogenesis of Lassa fever virus infection: I. Susceptibility of mice to recombinant Lassa Gp/LCMV chimeric virus. *Virology* 442(2):114–121.
19. Emonet SF, Garidou L, McGavern DB, de la Torre JC (2009) Generation of recombinant lymphocytic choriomeningitis viruses with trisegmented genomes stably expressing two additional genes of interest. *Proc Natl Acad Sci USA* 106(9):3473–3478.
20. Brooks DG, et al. (2006) Interleukin-10 determines viral clearance or persistence in vivo. *Nat Med* 12(11):1301–1309.
21. Ejrnaes M, et al. (2006) Resolution of a chronic viral infection after interleukin-10 receptor blockade. *J Exp Med* 203(11):2461–2472.
22. Barber DL, et al. (2006) Restoring function in exhausted CD8 T cells during chronic viral infection. *Nature* 439(7077):682–687.
23. Wherry EJ (2011) T cell exhaustion. *Nat Immunol* 12(6):492–499.
24. Teijaro JR, et al. (2013) Persistent LCMV infection is controlled by blockade of type I interferon signaling. *Science* 340(6129):207–211.
25. Wilson EB, et al. (2013) Blockade of chronic type I interferon signaling to control persistent LCMV infection. *Science* 340(6129):202–207.
26. Frebel H, et al. (2012) Programmed death 1 protects from fatal circulatory failure during systemic virus infection of mice. *J Exp Med* 209(13):2485–2499.
27. García-Sastre A, Biron CA (2006) Type 1 interferons and the virus-host relationship: A lesson in détente. *Science* 312(5775):879–882.
28. Zhou S, et al. (2010) Induction and inhibition of type I interferon responses by distinct components of lymphocytic choriomeningitis virus. *J Virol* 84(18):9452–9462.
29. Clingan JM, Ostrow K, Hosiawa KA, Chen ZJ, Matloubian M (2012) Differential roles for RIG-I-like receptors and nucleic acid-sensing TLR pathways in controlling a chronic viral infection. *J Immunol* 188(9):4432–4440.
30. Macal M, et al. (2012) Plasmacytoid dendritic cells are productively infected and activated through TLR-7 early after arenavirus infection. *Cell Host Microbe* 11(6): 617–630.
31. Walsh KB, et al. (2012) Toll-like receptor 7 is required for effective adaptive immune responses that prevent persistent virus infection. *Cell Host Microbe* 11(6):643–653.
32. Wang Y, et al. (2012) Timing and magnitude of type I interferon responses by distinct sensors impact CD8 T cell exhaustion and chronic viral infection. *Cell Host Microbe* 11(6):631–642.
33. Tabeta K, et al. (2006) The Unc93b1 mutation 3d disrupts exogenous antigen presentation and signaling via Toll-like receptors 3, 7 and 9. *Nat Immunol* 7(2):156–164.
34. Binder D, Fehr J, Hengartner H, Zinkernagel RM (1997) Virus-induced transient bone marrow aplasia: Major role of interferon-alpha/beta during acute infection with the noncytopathic lymphocytic choriomeningitis virus. *J Exp Med* 185(3):517–530.
35. Iannacone M, et al. (2008) Platelets prevent IFN-alpha/beta-induced lethal hemorrhage promoting CTL-dependent clearance of lymphocytic choriomeningitis virus. *Proc Natl Acad Sci USA* 105(2):629–634.
36. Yamane A, et al. (2008) Interferon-alpha 2b-induced thrombocytopenia is caused by inhibition of platelet production but not proliferation and endomitosis in human megakaryocytes. *Blood* 112(3):542–550.
37. Pozner RG, et al. (2010) Junín virus infection of human hematopoietic progenitors impairs in vitro proplatelet formation and platelet release via a bystander effect involving type I IFN signaling. *PLoS Pathog* 6(4):e1000847.
38. Kunz S (2009) The role of the vascular endothelium in arenavirus haemorrhagic fevers. *Thromb Haemost* 102(6):1024–1029.
39. Carrero JA, Calderon B, Unanue ER (2004) Type I interferon sensitizes lymphocytes to apoptosis and reduces resistance to Listeria infection. *J Exp Med* 200(4):535–540.
40. Trinchieri G (2010) Type I interferon: Friend or foe? *J Exp Med* 207(10):2053–2063.
41. Flatz L, et al. (2010) T cell-dependence of Lassa fever pathogenesis. *PLoS Pathog* 6(3): e1000836.
42. Meulen Jt, et al. (2004) Old and New World arenaviruses share a highly conserved epitope in the fusion domain of the glycoprotein 2, which is recognized by Lassa virus-specific human CD4+ T-cell clones. *Virology* 321(1):134–143.
43. Pober JS, Sessa WC (2007) Evolving functions of endothelial cells in inflammation. *Nat Rev Immunol* 7(10):803–815.
44. Baccala R, et al. (2012) Anti-IFN-α/β receptor antibody treatment ameliorates disease in lupus-predisposed mice. *J Immunol* 189(12):5976–5984.